Cold collisions between alkali metals and alkaline-earth metals in the heteronuclear atom-ion system Li + Ba⁺

Dibyendu Sardar[1,*] and Somnath Naskar [2,†]

[1]*JILA, University of Colorado, Boulder, Colorado 80309, USA*
[2]*Department of Physics, Jogesh Chandra Chaudhuri College, Kolkata 700033, India*

In a recent experiment [P. Weckesser *et al.*, Nature (London) **600**, 429 (2021)], the quantum *s*-wave regime was attained for an alkali-metal and alkaline-earth atom-ion combination (LiBa⁺). We investigate possible outcomes from the interaction of this ion-atom pair at quantum regimes from a theoretical point of view. For this purpose, Born-Oppenheimer potential energy surfaces are constructed for the three lowest dissociation channels of the (Ba-Li)⁺ molecular system using a multireference configuration interaction electronic-structure calculation. We present elastic, spin-exchange (SE), and diffusion cross sections in different energy regimes. The collisional properties of this system are calculated in terms of the scattering phase shifts and scattering cross sections, and the semiclassical behavior at a relatively high energy limit is also examined. For SE collisions, phase locking is obtained towards lower partial waves.

I. INTRODUCTION

Synthesization of cold molecules or molecular ions from cold atoms or ion-atom (IA) mixtures is a major research topic in the domain of atomic and molecular physics. Amidst several methods available for the formation of cold molecules, two of the most important methods are photoassociation (PA) [1] and magnetoassociation (MA) [2] at ultracold temperatures. The rich structure of the cold molecular ions purveys many new applications and research directions from precision measurements to quantum computing and quantum simulation [3]. In the realm of ultracold temperatures, where the de Broglie wavelength becomes comparable to or longer than the particle size or interparticle separation, such systems exhibit several quantum effects, for example, resonances and tunneling. This provides an opportunity for understanding controlled chemical reactions at ultracold energies.

The IA combination has received considerable attention and impressive evolution over the past decade. By harnessing the mutual interaction between the two quantum systems, namely, an atom and an ion, an integrated IA hybrid setup has been formed [4]. The interaction between an ionic species and a neutral particle is governed by the electrical induction process. It can be understood in terms of the interaction of the charge of an ion with the electrons of neutral atoms. Generally, these induction-controlled interactions are stronger compared to van der Waals types of interactions. Whenever a neutral atom comes near an ion, the atom is polarized by the electric field of the ion, i.e., the ion induces a dipole moment in the atom and thereby interacts with it. The IA interaction potential is given by $V(R) = -C_4/R^4$, where C_4 is the induction coefficient which depends on the static polarizability of the atom. These hybrid systems may offer a new platform for investigating elastic, inelastic, and reactive collisions between ions and atoms at low temperatures. Ion-atom collisions are important to understand charge transport phenomena [5], IA bound states [6], cold-molecular ions [7], etc. Recently, SE reaction processes have been investigated in IA colliding systems [8,9]. It has been proposed that controlled IA cold collisions may be used for future quantum information processing [10].

Over the past couple of years, there have been several studies on alkali-metal atom and alkaline-earth ion systems. The frequent use of alkaline-earth ionic species in most of the hybrid IA experiments is due to its suitability for laser cooling, which aids in achieving low IA collision energies. Some of the important and well-studied heteronuclear alkali-metal–alkaline-earth IA systems are Na-Be⁺ [11], Na-Ca⁺ [12], Rb-Ca⁺ [13], Rb-Yb⁺ [14], Li-Yb⁺ [15], K-Mg⁺ [16], and Cs-Mg⁺ [17]. Apart from heteronuclear IA combination, studies have also been made on homonuclear alkaline-earth–alkaline-earth systems, e.g., Be-Be⁺ [18], Mg-Mg⁺ [19], and Yb-Yb⁺ [20]. In most of these studies, cold collisions, the formation of molecular ions, and Feshbach resonances (FRs) are the major goals accomplished by either PA or MA; however, experimental realization of such important phenomena is yet to be achieved.

A usual experimental obligation of IA systems towards achieving low temperatures is that the ions cannot be cooled to μK or sub-μK temperatures due to the presence of inherent trap-induced micromotion. The heavier the ion is, the less micromotion there is and thereby the more suitable it is for cooling. Theoretically, it has been proposed that the lowest-energy regimes may be reached for an IA combination having the highest mass ratio [21]. In a very recent experiment, the quantum regime was reached with an alkali-metal–alkaline-earth IA system having a mass ratio of approximately 23–28.

---

*Corresponding author: chem.dibyandu.sardar@gmail.com
†snaskar@jogeshchaudhuricollege.org

The Li-Yb$^+$ system [22,23] is an early workhorse in this effort. In this system the s-wave regime is attained at a collision energy of $8.6k_B$ μK, where k_B is the Boltzmann constant. The investigation comprises the spin dynamics of a single trapped Yb$^+$ ion in a cold spin-polarized bath of Li atoms without any signature of FR in such an energy limit.

In the experiment by Weckesser *et al.* [24], FRs were detected in the case of a single trapped ^{138}Ba$^+$ ion and ^{6}Li atoms. For this system, a total number of 11 FR were identified out of which four were due to s-wave FR for different values of the tunable magnetic field. This number of observed resonances is mainly due to the additional interaction, namely, the second-order spin-orbit coupling (SOC). This coupling mixes internal states (m_F) with the rotational motion (l, m_l), causing the increased number of resonances [25] in the ^{6}Li-^{138}Ba$^+$ system. These encouraging results provide deeper insight into IA interactions, thereby paving a way to explore complex many-body systems and quantum simulations. For low-energy domains, especially in the μK or sub-μK regime, quantum-mechanical scattering calculations are inevitable to describe the IA interactions, where the scattering is characterized by quantum phase shift in the scattered wave function. Quantities such as scattering length in the s-wave regime and scattering cross section can be calculated in terms of this quantum phase shift. At a larger energy limit $E \geqslant 1k_B$ mK, a simpler semi-classical description is useful.

In most of the alkali-metal–alkaline-earth IA systems the choice of initial collision channel lies at the excited asymptote with a lighter-atom–heavier-ion combination. This choice is a matter of experimental compulsion as a heavier ion is favorable for cooling, as discussed earlier. A disadvantage of this situation is that the excited asymptote is short lived and decays to the ground asymptotic channel through radiative charge exchange collisions. As an interesting exception, however, the collisional asymptote of Li-Ba$^+$ is energetically lower than that of Li$^+$-Ba. Thus, the initial collision channel for the (BaLi)$^+$ IA system is naturally chosen to be the Li-Ba$^+$ ground collisional asymptote [24], which is free from the radiative charge-transfer loss mechanism and therefore has a much much longer lifetime compared to other IA systems. Along with this, as discussed earlier, this particular IA system allows an ultracold window to study controllable collision resonances. Thus, from an experimental point of view, compared to other IA systems, the ^{6}Li-^{138}Ba$^+$ system turns out to be an extremely novel one.

Depending on the orientation of the electronic spin located at each species in their ground state, two molecular potentials are formed: a singlet Sigma ($X\,^1\Sigma^+$) and a triplet Sigma ($a^3\Sigma^+$) at the short-range IA internuclear separation. These two potentials offer elastic collisions and inelastic SE collisions in low-energy regimes. In the presence of second-order SOC, the total spin projection is not conserved during collision, tendering the possibility of spin relaxation (SR) [26]. The SR competes with the SE process and weakens the spin control of the system. In the ultracold regime, however, the rate of SR becomes much slower [27] than the Langevin collision rate and the former is strongly suppressed. While studying SE collisions at low energies, partial-wave phase locking (PWPL) [27] has been observed where the difference

in the quantum phase shifts due to the two potentials is found to be independent of the partial-wave quantum number.

In this paper our theoretical investigation with the ^{6}Li-^{138}Ba$^+$ system is organized as follows. In Sec. II we exploit the *ab initio* method for calculating electronic structures of the (BaLi)$^+$ system. We present in Sec. III a detailed prospective scheme to realize FR in the system. Section IV is devoted to investigating IA collisions employing the electronic states $X\,^1\Sigma^+$ and $a\,^3\Sigma^+$ which go asymptotically to the same dissociation limit. We determine the collisional properties in terms of scattering phase shift and scattering cross section and attempt to justify the semiclassical behavior at a relatively high-energy limit. We also study the PWPL effect at low energies. We summarize in Sec. V.

II. *AB INITIO* CALCULATION

In this section we describe *ab initio* calculations to construct the potential energy surface of a heteronuclear IA system (BaLi)$^+$. The *ab initio* calculations are performed using the MOLPRO 2012.1 software package [28]. The electronic-structure calculations are performed by the multireference configuration interaction (MRCI) with additional Davidson correction that approximately accounts for the size consistency and higher excitations.

The ground-state electronic configurations of the Ba and Li atoms are expressed as $[\mathrm{Kr}]_{36}4d^{10}5s^25p^66s^2$ and $1s^22s^1$, respectively. The lighter candidate lithium is described by the correlation consistent polarized valence quadruple-ζ basis set with augmenting functions, e.g., aug-cc-pwCVQZ [29]. For the barium atom, a pseudopotential-based correlation consistent polarized weighted core valence triple-ζ basis set (cc-pwCVTZ-PP) is used [30], where the inner core electrons are described by the Stuttgart-Köln effective core potential ([ECP46MDF] [31]).

The inner core electrons of Ba are replaced by core potentials ECP46MDF, leaving eight subvalence ($5s5p$) and two valence ($6s$) electrons in the outer shell. Therefore, the effective number of molecular orbitals of (BaLi)$^+$ is reduced to seven, where orbitals $5s5p6s$ and $1s2s$ appear from the Ba and Li atoms, respectively. These occupied molecular orbitals are expressed as $(5a_1, 1b_1, 1b_2, 0a_2)$ or $(5, 1, 1, 0)$ in the C_{2v} Abelian point group symmetry used by MOLPRO. We define an active space denoted by $(9, 4, 4, 1)$ in which the $5d6p$ atomic orbitals of Ba and $2p$ atomic orbitals of Li are included in the reference space. The doubly occupied orbitals are set to $(3, 1, 1, 0)$. The energies of the molecular orbitals on this active space are calculated in the following way: Initially, the spin-restricted optimized Hartree-Fock molecular orbitals are used as solutions for the complete-active-space self-consistent field (CASSCF) problem. Thereafter, a dynamical correlation is carried out by internally contracted the MRCI with single and double excitations being taken relative to this CASSCF reference wave functions where the $5s5p$ atomic orbitals of Ba and the $1s$ orbital of Li are correlated. The above-described method is used in constructing final potential energy surfaces; nevertheless, we further verify the validity of approach.

It is a difficult task to estimate the uncertainty of *ab initio* calculations, especially for a many-electron system including a heavy atom. However, before proceeding to describe the

TABLE I. First ionization potential values of Li and Ba in eV.

Atom	IP (eV)	Expt.	Theory
Li	5.393	5.4 ± 0.2[a]	5.39[a]
Ba	5.057	5.3 ± 0.3[a]	5.0[a]

[a]From Ref. [32].

potential energy curves of the (BaLi)$^+$ molecular system, we compare the results of our computed atomic components to the available experimental data. The comparison is accomplished in terms of the first ionization potential (IP) of Ba and Li, including static electric dipole polarizability α for both neutral and charged components of barium and lithium atoms, as shown in Tables I and II. In our current method of calculation, the predicted ionization potentials of Li and Ba agree well with previously reported experimental and theoretical values with an error of less than 1%. With regard to the static electric dipole polarizability of the ground-state Li, our calculated value is in good agreement with the experimental result [33] but differs by $0.3a_0^3$ from the theoretical value [15]. The calculated value of α for Li$^+$ is $0.192a_0^3$ and the experimental value is 0.188 ± 0.002 [34]. As for the Ba and Ba$^+$ components, the static polarizabilities are in good agreement with experimental and theoretical values. The harmony of these results with the literature values can impart a reliable description of the diatom molecular ion (BaLi)$^+$ using our current level of theory and the basis sets. Some of the potential energy curves for the ground and excited states of the (BaLi)$^+$ molecular system are shown in Fig. 1. The spectroscopic parameters associated with these potentials are represented in Table III in terms of the equilibrium bond length R_e and depth of the well D_e. All the equilibrium bond lengths of these molecular electronic states are expressed in angstroms whereas the D_e values are in cm^{-1}. For this alkali-metal–alkaline-earth IA system, depending on the location of the positive charge at the dissociation limit, two possible IA combinations may arise, either an alkali-metal ion and alkaline-earth atom or an alkali-metal atom and alkaline-earth ion. The corresponding dissociation threshold will be energetically different depending on the ionization potential of the atom involved. In the latter case, there are two unpaired valence electrons in each

TABLE II. Static electric dipole polarizability values of Li (Li$^+$) and Ba (Ba$^+$) in atomic units.

Atom or ion	α (a.u.)	Expt.	Theory
Li	164.30	164 ± 3.4[a]	164.0[b]
Li$^+$	0.192	0.188 ± 0.002[c]	0.190[b]
Ba	267.74	268 ± 6[d]	268.19[e]
Ba$^+$	124.22	123.88 ± 5[f]	124.26 ± 1[g]

[a]From Ref. [33].
[b]From Ref. [15].
[c]From Ref. [34].
[d]From Ref. [35].
[e]From Ref. [36].
[f]From Ref. [37].
[g]From Ref. [38].
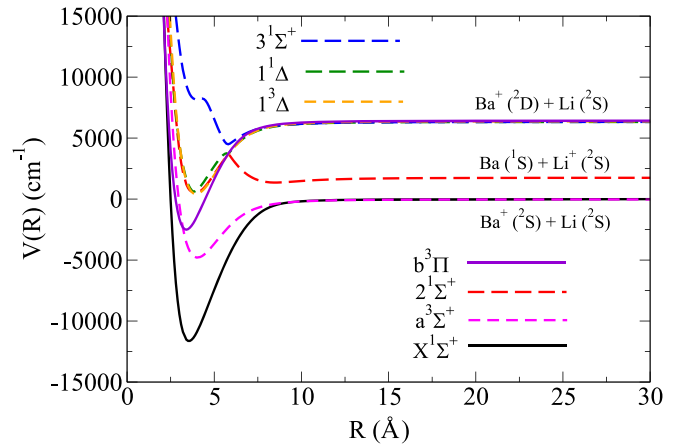

FIG. 1. Adiabatic potential energy curves of three lowest dissociation channels of the (BaLi)$^+$ molecular system plotted as a function of IA internuclear separation. The energies are in units of the wave number.

species that result in singlet and triplet molecular potential curves.

For the case of (BaLi)$^+$, the possible asymptotic arrangements are given as Ba$^+$-Li and Ba-Li$^+$ depending on the localization of the positive charge of either the Ba atom or the Li atom. Since the first ionization potential of Ba is lower than that of Li, as compared in Table I, the Ba$^+$-Li arrangement is in the absolute ground-state asymptote of the (BaLi)$^+$ system. Due to this feature of the ground-state asymptote, this system is significantly different compared to other heteronuclear alkali-metal–alkaline-earth IA systems, as mentioned earlier. In the ground-state asymptotic arrangement of the (BaLi)$^+$ system, the interaction occurs between the ground-state Ba$^+$ ion and the ground-state Li atom, which are both open shells. Two electronic states $X\,^1\Sigma^+$ and $a\,^3\Sigma^+$ appear as a result of this interaction. The features of these two states need to be explained as we use them frequently in the domain of cold collisions. The singlet Σ state is strongly bound, having binding energy equal to $11\,627$ cm^{-1}, and the equilibrium position is located at $3.55a_0$. On the other hand, the triplet Σ state is bound by 4675 cm^{-1} and the equilibrium distance is equal to $4a_0$. We compare our results to the available data from Śmiałkowski and Tomza [39] only for the singlet Σ state. We note that our calculated equilibrium bond length and depth of the well are in excellent agreement with those Ref. [39] with

TABLE III. Spectroscopic constants for some lowest molecular electronic states of (BaLi)$^+$ expressed in terms of equilibrium bond length and depth of the well.

Molecular state	R_e (Å)	D_e (cm^{-1})
$X\,^1\Sigma^+$	3.55	11627
$a\,^3\Sigma^+$	4.00	4784
$2\,^1\Sigma^+$	4.01	1206
$3\,^1\Sigma^+$	5.80	1833
$2\,^3\Sigma^+$	3.96	5961
$b\,^3\Pi$	3.40	8935
$1\,^1\Delta$	3.80	5729

an uncertainty less than 1% and we accept this as adequate. In addition, our calculated potentials are the same as those of Ref. [24] if one uses the conversion factor 1 Å = 1.889 73a_0.

The two other dissociating thresholds conceive the electronic states $2\,^1\Sigma^+$, $3\,^1\Sigma^+$, $1\,^3\Delta$, $b\,^3\Pi$, and $1\,^1\Delta$. The asymptotes $Ba(^1S) + Li^+(^2S)$ and $Ba^+(^2D) + Li(^2S)$ lie above the ground-state asymptote by energies of approximately $1740\ \mathrm{cm^{-1}}$ and approximately $6300\ \mathrm{cm^{-1}}$, respectively. There is one noticeable pattern in Fig. 1. The electronic state $a\,^3\Sigma^+$ correlated to the ground-state asymptote crosses the state $b\,^3\Pi$ at a location near $3.2a_0$. This curve crossing facilitates a large spin-orbit coupling which plays an important role in the spin nonconserving scattering phenomena. In the following we discuss the method and the result of the spin-orbit matrix-element calculation.

Spin-orbit matrix element

The spin-orbit-coupling matrix elements ξ^{so} between two molecular states $a\,^3\Sigma^+$ and $b\,^3\Pi$ can be expressed as

$$\xi^{so} = \langle a\,^3\Sigma^+|H_{so}|b\,^3\Pi\rangle, \tag{1}$$

where H_{so} is the spin-orbit Hamiltonian which is either the Breit-Pauli operator or the spin-orbit pseudopotential. The matrix elements of the spin-orbit-coupling Hamiltonian are evaluated by exploiting the wave functions of electronic states $a\,^3\Sigma^+$ and $b\,^3\Pi$. The calculations of the electronic wave functions are carried out using MOLPRO. The spin-orbit-coupling constant λ associated with the spin-orbit matrix element is

$$\lambda(R) = \frac{2}{3} \frac{|\langle a^3\Sigma^+|H_{so}|b^3\Pi\rangle|^2}{V_{b^3\Pi}(R) - V_{a^3\Sigma^+}(R)}. \tag{2}$$

It is noteworthy that the sign of the originally calculated spin-orbit matrix elements is not well defined as the phase of the corresponding wave functions is arbitrary. This means that the phase of the coupling matrix elements strictly depends on the signs of the successive calculations performed: It starts with the relative signs of the molecular orbitals optimized by CASSCF, which are used in the MRCI calculations of the triplet $a\,^3\Sigma^+$ and $b\,^3\Pi$ states, providing MRCI eigenvectors, each defined with a phase factor. The spin-orbit integrals are calculated using the CASSCF molecular orbitals (with their signs) and the spin-orbit matrix elements combine the configuration interaction eigenvectors with the integrals. Each of the calculations performed on a given geometry is thus correct, but the relative signs between different geometries are arbitrary.

In Fig. 2(b) we plot the absolute value of the spin-orbit matrix element in $\mathrm{cm^{-1}}$ as a function of internuclear separation between the electronic states $a\,^3\Sigma^+$ and $b\,^3\Pi$. We note that the matrix element decreases exponentially with an increase in IA distance. In Fig. 2(a) we plot the two concerned potentials as a function of IA distance showing the crossing between the curves. The curve crossing occurs at a distance $R = 3.2a_0$. The value of the coupling constant near the curve crossing is approximately $20\ \mathrm{cm^{-1}}$. Then it decreases rapidly with IA distance and finally for $R > 5.6a_0$ it reaches nearly a constant value less than $1\ \mathrm{cm^{-1}}$, as shown in Fig. 2(c). We note that the value of λ_{so} near the equilibrium distance of the $a\,^3\Sigma^+$ potential is comparable to that of the $(LiYb)^+$ system.
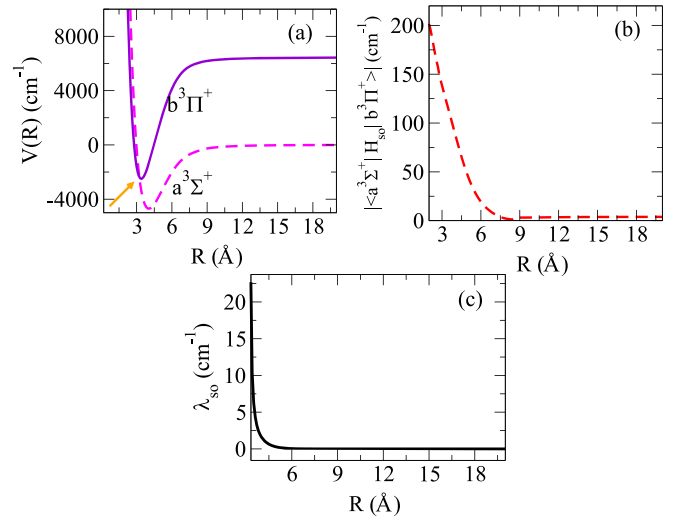

FIG. 2. (a) Potentials $a\,^3\Sigma^+$ and $b\,^3\Pi$ with the arrow indicating the crossing between these two potentials. Also shown are (b) the spin-orbit matrix element and (c) the spin-orbit coupling constant.

III. CONSTRUCTION OF HYPERFINE POTENTIALS: PROSPECTIVE FESHBACH RESONANCES

Experimentally, the ion Ba^+ is prepared in an incoherent mixture spin state $|6S_{1/2}; s^{Ba^+} = 1/2, m_s^{Ba^+} = \pm 1/2\rangle$ and the atom Li is considered in the hyperfine state $|f_{Li} = 1/2, m_f^{Li} = -1/2\rangle$. Then the ion and the atom are allowed to interact, resulting a number of FRs out of which four are detected as s-wave resonances. In this section we introduce a brief description of the construction of hyperfine potentials that could be used to characterize the s-wave FR.

Channel classification

The ion $^{138}Ba^+$ has vanishing nuclear spin ($i_1 = 0$) with electronic spin $s_1 = 1/2$. One can label the hyperfine sublevels as $|f_1 = 1/2, m_{f_1} = \pm 1/2\rangle$. On the other hand, ^6Li has nuclear spin $i_2 = 1$ with hyperfine quantum number $f_2 = 3/2$ and $1/2$; these two hyperfine levels are separated by an energy of 228.2 MHz (approximately 10.952 mK). In the presence of an external magnetic field, the projection M_J of the total angular momentum $\mathbf{J} = \mathbf{f}_1 + \mathbf{f}_2 + \mathbf{l}$ remains a good quantum number during a collision event. In addition, states with a different orbital angular momentum $\mathbf{l}$ characterizing different partial waves are decoupled if one neglects the anisotropic spin-spin interaction, making l and its projection m_l conserved. Under this condition, $M_f = m_{f_1} + m_{f_2}$ will also be conserved. Here we restrict our discussion to the subspace of a partial wave $l = 0$ including M_f as a constant. We constrict the collision within the subblock $M_f = 1/2$ as it represents the lowest-energy channel state. In the absence of a magnetic field $B = 0$ and for $M_f = 1/2$, there are four possible channels constituting the asymptotic or uncoupled basis $|f_1 m_1, f_2 m_2\rangle$, as listed in Table IV.

In the absence of a magnetic field, the hyperfine interaction is diagonal in the basis $|f_1 m_1, f_2 m_2\rangle$. In this condition, since both f^2 and l^2 are conserved, another useful basis that may be used is the coupled hyperfine basis $|(f_1 f_2) f m_f\rangle$. One can use this basis in the presence of a weak magnetic field considering

TABLE IV. Four asymptotic channels for $M_F = 1/2$ of the $(^{138}\text{Ba} \text{-} {}^6\text{Li})^+$ system.

Channels	(f_1, m_{f_1})	(f_2, m_{f_2})	E^∞ (mK)
1	(1/2, 1/2)	(1/2, −1/2)	0
2	(1/2, −1/2)	(1/2, 1/2)	0
3	(1/2, 1/2)	(3/2, −1/2)	10.952
4	(1/2, −1/2)	(3/2, 1/2)	10.952

a perturbative treatment with a very small Zeeman interaction. In simplified notation, we denote this basis by $|b\rangle$. Now in the presence of a magnetic field, let the basis that diagonalizes both Zeeman and hyperfine terms be $|\tilde{b}\rangle$. On diagonalization, one obtains eigenvalues that define the threshold energies of the channels and the eigenvectors that are related to the basis $|b\rangle$ through some linear transformation as

$$|b\rangle = \sum_{\tilde{b}} \langle \tilde{b}|b\rangle |\tilde{b}\rangle. \tag{3}$$

The matrix elements of the central potential in the coupled basis can be given as

$$
\begin{aligned}
&\langle (f_1 f_2) f m_f |V^c|(f_1' f_2') f' m_f' \rangle \\
&= \sum_{S,I,M_S,M_I} V_S \langle (f_1 f_2) f m_f |SM_S, IM_I \rangle \\
&\quad \times \langle SM_S, IM_I|(f_1' f_2') f' m_f' \rangle.
\end{aligned} \tag{4}
$$

Here $|SM_S, IM_I\rangle$ is the adiabatic basis and the central potential is diagonal in this basis with eigenvalues V_S. The central potential can be written as $V^c = V_0(r)P_0 + V_1(r)P_1$, where $V_0(r)$ and $V_1(r)$ correspond to the singlet $X\,^1\Sigma^+$ and triplet $a\,^3\Sigma^+$ states, respectively, and P_0 and P_1 are the corresponding projections. Here the adiabatic basis and the coupled asymptotic basis are related through the transformation matrix elements

$$
\begin{aligned}
&\langle SM_S, IM_I|(f_1 f_2) f m_f \rangle \\
&= C^{S,I,f}_{M_S,M_I,m_f} \sqrt{(2f_1 + 1)(2f_2 + 1)(2S + 1)(2I + 1)} \\
&\quad \times \begin{Bmatrix} s_1 & i_1 & f_1 \\ s_2 & i_2 & f_2 \\ S & I & f \end{Bmatrix} \left(\frac{1 + (1 - \delta_{f_1 f_2})(-1)^{S+I+l}}{\sqrt{2 - \delta_{f_1 f_2}}} \right), \tag{5}
\end{aligned}
$$

where $C^{S,I,f}_{M_S,M_I,m_f}$ is the Clebsch-Gordan (CG) coefficient and $m_f = M_S + M_I$. The quantity in the curly bracket is known as the 9-j symbol [40]. Considering these transformations, we present the variation of channel energies with magnetic field in Fig. 3, where the numbers inside the plot indicate the indices of the channels. In Fig. 4 we present four diagonal potentials in the short-range regime as a function of internuclear separation R (Bohr) for a particular magnetic field $B = 100$ G. The asymptotic long-range part of the potentials is shown in the inset of Fig. 4 and the energy of the said channels increases from channel 4 to channel 1 as a function of magnetic field. With this primary knowledge at hand, one can study the FR in the $(\text{BaLi})^+$ system.
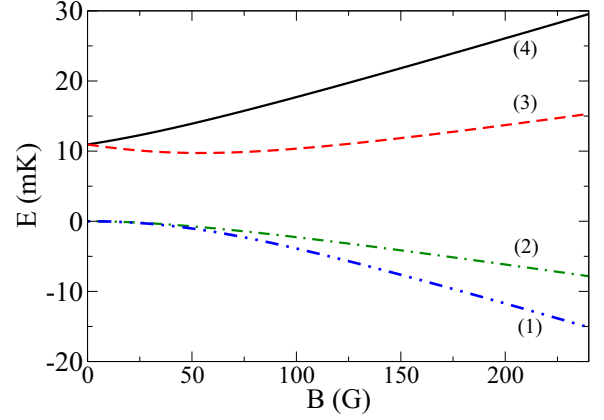

FIG. 3. Variation of energy of the four channels as a function of magnetic field.

IV. COLD COLLISIONS

Experimentally, the $^{138}\text{Ba}^+$ ion and ^6Li atom are prepared in their electronic ground state ^2S, which corresponds to the lowest-energy dissociation channel $[\text{Ba}^+(^2S) + \text{Li}(^2S)]$ of the $(\text{BaLi})^+$ system. Therefore, the charge exchange collision requiring a photon or enough collision energy corresponding to an excitation of the system for the next dissociation limit is strongly suppressed. Herein, we consider mainly low-energy processes in the domain of energy of μK to sub-mK and therefore we restrict our discussion to the area of elastic scattering and SE processes.

A. Elastic collision

A $^{138}\text{Ba}^+$ ion colliding elastically with a ^6Li neutral atom in its ground state is associated with the asymptote $[\text{Ba}^+(^2S) + \text{Li}(^2S)]$ where both potentials $X\,^1\Sigma^+$ and $a\,^3\Sigma^+$ will be relevant. Applying the method of partial-wave decomposition in the total wave function, the time-independent
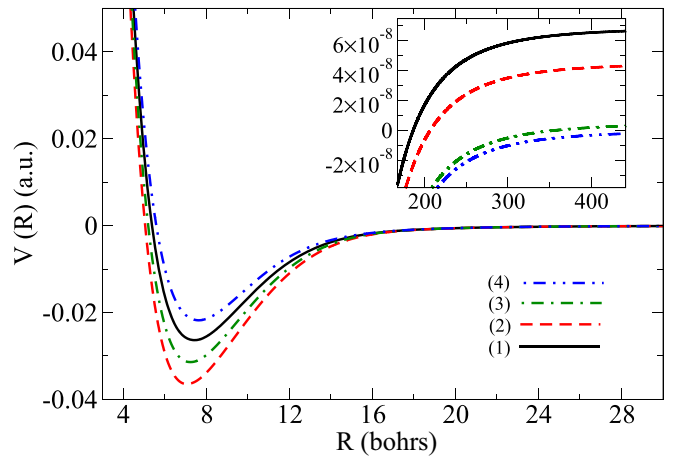

FIG. 4. Variation of four diagonal potentials of the $(\text{BaLi})^+$ system as a function of IA distance at short range for a particular magnetic field $B = 100$ G. The corresponding asymptotes are shown in the inset.
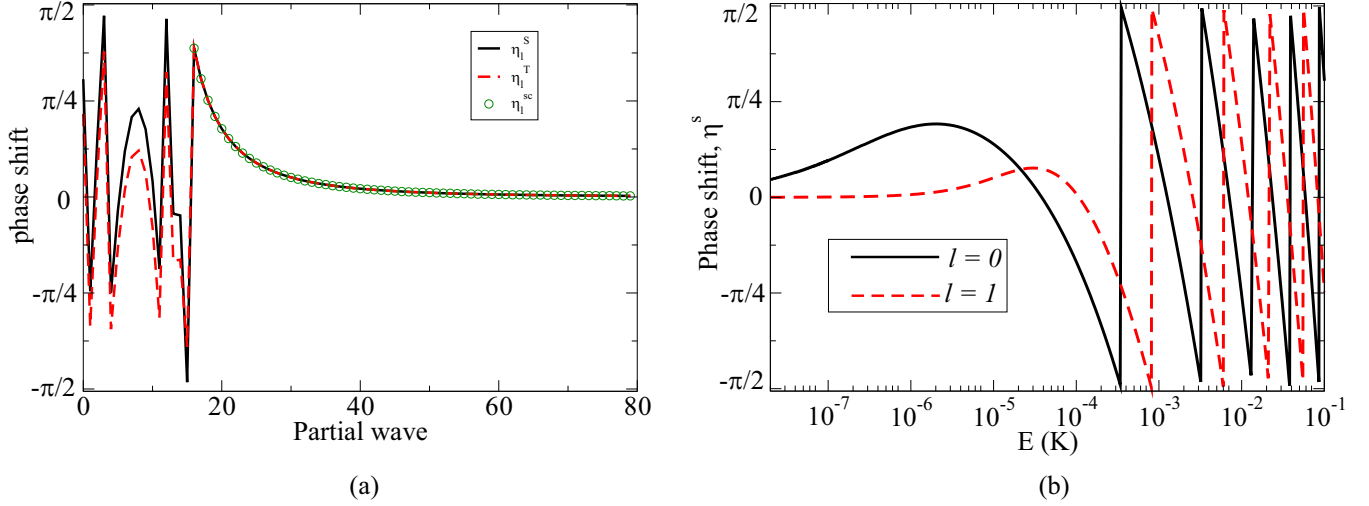
FIG. 5. (a) Quantum and semiclassical phase shifts plotted as a function of partial waves for the potentials $X^{1}\Sigma^{+}$ and $a^{3}\Sigma^{+}$. (b) Quantum phase shifts shown for the partial waves $l = 0, 1$ as a function of energy only for the $X^{1}\Sigma^{+}$ state.

Schrödinger equation at a given collision energy E is given by

$$\left(\frac{d^{2}}{dR^{2}} + k^{2} - 2\mu V_{S,T}(R) - \frac{l(l+1)}{R^{2}}\right)y_{E,l}^{S,T}(R) = 0, \quad (6)$$

where the wave number $k = \sqrt{2\mu E}/\hbar$, μ is the reduced mass of the colliding IA pair, and l is the partial wave. The quantities V_{S} and V_{T} are related to the potentials $X^{1}\Sigma^{+}$ and $a^{3}\Sigma^{+}$, respectively. The long-range part of the potential is approximated as $V_{S,T}(R) = -(\frac{C_{4}}{R^{4}} + \frac{C_{6}}{R^{6}})$, where $C_{4} = \frac{1}{2}q^{2}\alpha_{Li}$, the coefficient related to the dipole polarizability (α_{Li}) of the Li atom. The quadrupole polarizability β_{Li} is associated with the C_{6} coefficient $C_{6} = \frac{1}{2}q^{2}\beta_{Li}$. In this work we use $\alpha_{Li} = 164.1$ a.u. and $\beta_{Li} = 1424$ a.u. The short-range and long-range parts of the potentials are joined smoothly by a cubic spline algorithm. In the asymptotic limit, the wave function can be expressed in terms of the Bessel $[j_{l}(kr)]$ and Neumann $[n_{l}(kr)]$ functions as

$$y_{E,l}^{S,T}(R) = kR[j_{l}(kr)\cos\eta_{l}^{S,T} - n_{l}(kr)\sin\eta_{l}^{S,T}], \quad (7)$$

where η_{l}^{S} and η_{l}^{T} are the phase shifts associated with the potentials $X^{1}\Sigma^{+}$ and $a^{3}\Sigma^{+}$, respectively. Equation (6) is solved numerically by the Numerov-Cooley method using the three-point recursion relation. The details of this method are discussed in Ref. [19].

In Fig. 5(a) we present a plot of phase shifts by varying the number of partial waves for the potentials $X^{1}\Sigma^{+}$ and $a^{3}\Sigma^{+}$, considering the collision energy $E = 0.1$ K. For a given large collision energy and high partial waves, the potentials $V_{S,T}(R)$ behave, to the leading term, as $-C_{4}/R^{4}$. Under this condition, one can find the semiclassical phase shift $\eta^{sc} \simeq (\pi\mu^{2}\alpha_{Li}/4\hbar^{4}) \times (E/l^{3})$. In the potentials we are concerned with, the semiclassical phase shift is in agreement with the quantum phase shifts for partial waves $l > 21$, as shown in Fig. 5 with collision energy $E = 0.1$ K. In Fig. 5(b) we show quantum phase shifts for the first two partial waves ($l = 0, 1$) as a function of collision energy for the potential energy surface $X^{1}\Sigma^{+}$. Note that the s-wave ($l = 0$) phase shift is dominant at very low energies whereas that of the p

wave decreases to zero. The phase shifts for both s and p waves change sign, indicating the presence of a pole where the scattering length diverges.

The scattering phase shift is associated with another physically measurable quantity, the scattering cross section. For a direct elastic collision, the cross sections $\sigma_{el}^{S,T}$ can be expressed in terms of scattering amplitude as [12]

$$\sigma_{el}^{S,T}(E) = \int |f_{S,T}|^{2}d\Omega = \frac{4\pi}{k^{2}}\sum_{l=0}^{\infty}(2l+1)\sin^{2}\left(\eta_{l}^{S,T}\right), \quad (8)$$

where $|f_{S,T}|^{2}$ are the scattering amplitudes associated with the singlet and triplet potentials of the $(BaLi)^{+}$ system and $d\Omega$ is the differential solid angle. At a relatively high collision energy, the cross sections are approximated by the semiclassical expression [41]

$$\sigma_{sc}(E) = \pi\left(\mu\alpha_{Li}^{2}/\hbar^{2}\right)^{1/3}(1 + \pi^{2}/16)E^{-1/3}. \quad (9)$$

Thus the plot of $\log\sigma_{sc}(E)$ vs $\log E$ is a straight line with slope $-1/3$ and the intercept is associated with dipole polarizability of the neutral Li atom.

We present total elastic scattering cross sections as a function of energy in kelvin for the $X^{1}\Sigma^{+}$ and $a^{3}\Sigma^{+}$ potentials in Figs. 6(a) and 6(b). The cross section includes the sum of the first 81 partial waves for the singlet Σ state and 65 partial waves for the triplet Σ state we consider. Here we note that the s-wave contribution is dominant in all the cases at energies corresponding to a temperature of 0.1 μK. For neutral alkali-metal atom systems, however, the s-wave contribution is dominant for energies around 100 μK [1]. This is due to the existence of the long-range polarization potential in the IA system as compared to the shorter-range van der Waals interactions between neutral atoms. As energy increases, more and more partial waves start to contribute to the total elastic scattering cross sections. In order to check the convergence for the sum over partial waves, we fit both plots linearly at the high-energy limit. The numerically calculated slope is quite close to the semiclassical theoretical value, confirming the
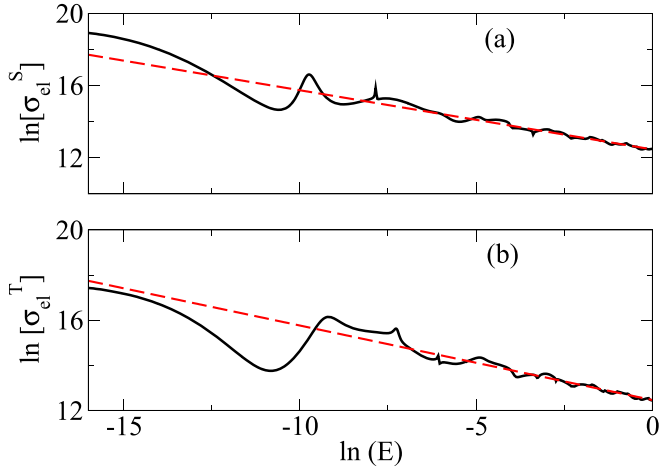
FIG. 6. Total elastic scattering cross sections are plotted as a function of collision energy in the log-log scale for the concerned singlet and triplet potentials in the panel-(a) and (b), respectively. The dashed line indicates the semiclassical fitting in cross sections.

convergence of partial-wave contributions in the total elastic scattering cross section.

B. Spin exchange collision

At short range, another possible outcome of the collisions between the ultracold ion ^{138}Ba$^+$ and atom ^{6}Li in their ground states is the SE collision. Under the SE interaction, the total spin projection is conserved along any axis. Due to this conservation property, if the ion and the atom are prepared with parallel electronic spins, they can interact only on the triplet potential and no SE takes place. On the other hand, if they are prepared with antiparallel spins, they interact on both singlet and triplet potentials, opening up a finite probability of SE. In the elastic as well as the degenerate internal state approximation, this scattering event is described in terms of the singlet and triplet scattering phase shifts. In the short

range, the inelastic SE cross section can be expressed as [12]

$$\sigma_{\text{SE}}(E) = \frac{\pi}{k^2} \sum_{l=0}^{\infty} (l+1) \sin^2\left(\eta_l^S - \eta_l^T\right). \tag{10}$$

In the Langevin regime of intermediate collisional energy, the SE cross section shows the classical Langevin behavior: $\sigma_L(E) \propto E^{-1/2}$. In Fig. 7(a) we show the SE cross section as a function of collision energy in kelvin in logarithm scale. The curve can approximately be fitted with a Langevin behavior (red dashed line) with slope $-1/2$ in the energy range 0.56–7.01 mK.

Due to the short-range nature of the SE interaction, the phase difference $\eta_l^S - \eta_l^T$ remains constant for a range of l values exhibiting PWPL [27]. For the (Ba-Li)$^+$ system, at a collisional energy of 10 mK, the maximum partial wave number l_{max} that contributes to $\sigma_{\text{SE}}(E)$ is found to be 7. We calculate $\sin^2(\eta_l^S - \eta_l^T)$ for these partial waves, which remains constant ($\mathscr{C}$) with 5.5% standard deviation as shown in Fig. 7(b). Thus, under the PWPL approximation, the expression for the SE cross section simplifies to

$$\sigma_{\text{SE}}(E) = \frac{3\pi\mathscr{C}}{2k^2} l_{\text{max}}(l_{\text{max}} + 1). \tag{11}$$

Conservation of the total spin projection is violated in the presence of SOC as it is not diagonal in the adiabatic basis $| SM_S, IM_I \rangle$. This leads to spin relaxation (SR). Thus the spin dynamics is governed by the competition of SE and SR. When the SR rate is significant compared to the Langevin collision rate, the spin controllability of the system is lost. However, in the ultracold regime, where the steady-state temperature is much lower than the hyperfine energy gap (10.952 mK), the SR rate becomes significantly lower.

C. Diffusion cross section

A charge or ion immersed in a dilute gas of atoms will diffuse through the stochastic scattering process. Therefore, the diffusion of the ion in a gas of atoms will change the position of the ion with time, resulting in a loss of forward
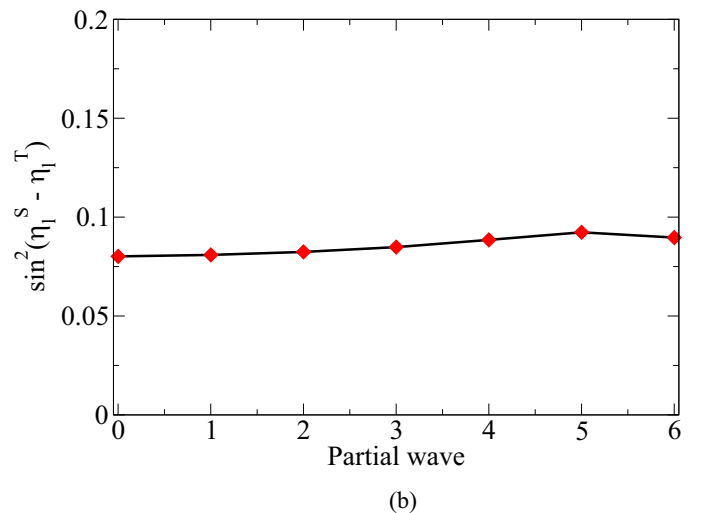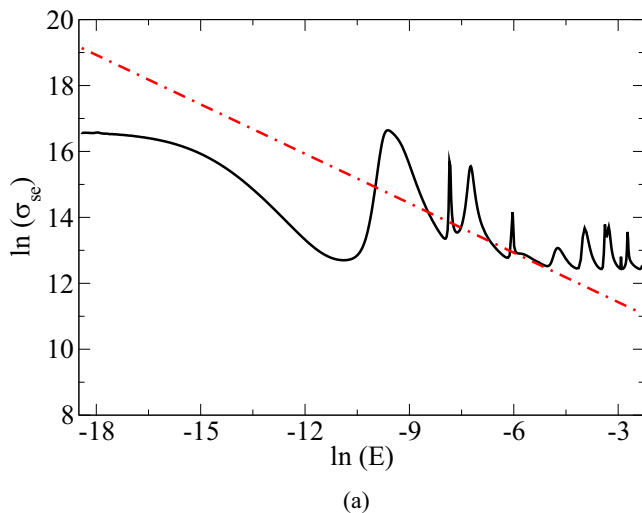

(a)

(b)

FIG. 7. Study of spin dynamics. (a) SE cross section as a function of energy in log-log scale. (b) Variation of the difference in singlet and triplet phase shifts as a function of l at energy $E = 10$ mK.
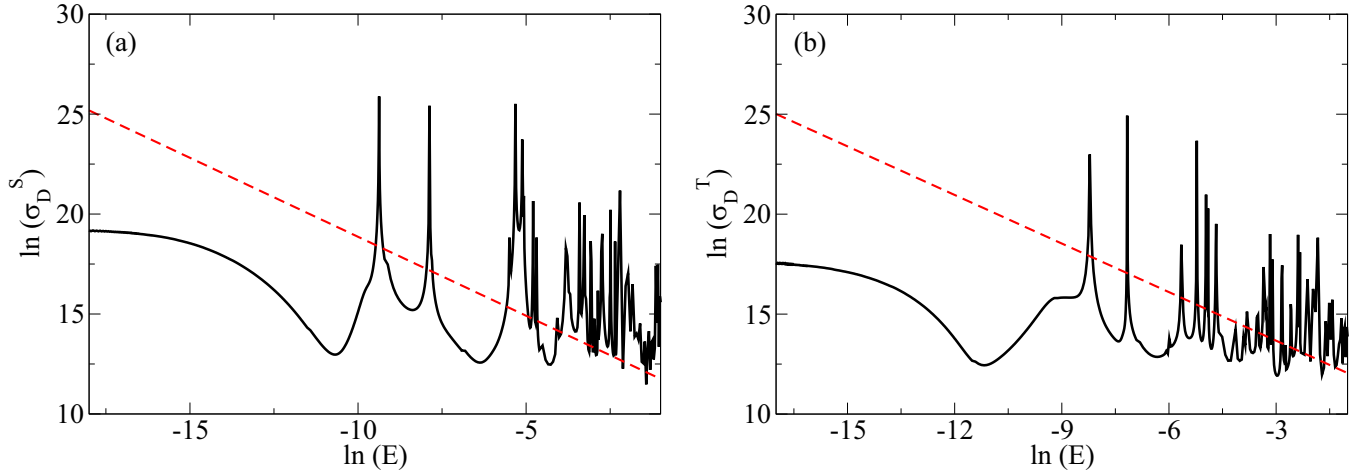
FIG. 8. Diffusion cross sections plotted as a function of energy in log-log scale for the potential $X\,^1\Sigma^+$ or $a\,^3\Sigma^+$. The red dashed lines indicate the Langevin behavior.

momentum of the ion [41–44]. This effect is quantified through the diffusion cross section or momentum transfer cross section. The diffusion of the ion is characterized by the diffusion coefficient. Diffusion occurs due to the binary collision of the ions with the atoms in the gas. The total diffusion cross section is associated with both elastic and inelastic contributions in the presence of atomic gases. It may be presumed that the inelastic diffusion cross sections will be small compared to the corresponding elastic quantities [45]. By eliminating inelastic phenomena, the diffusion cross section is associated with phase shifts for elastic collisions. The diffusion cross section for a heteronuclear IA pair approaching along a single potential curve $X\,^1\Sigma^+$ or $a\,^3\Sigma^+$ is given by [41]

$$\sigma_D^{S,T}(E) = \frac{4\pi}{k^2} \sum_{l=0}^{\infty} (2l+1) \sin^2\left(\eta_l^{S,T} - \eta_{l+1}^{S,T}\right). \qquad (12)$$

Using this equation, we evaluate diffusion cross sections $\sigma_D^{S,T}$ for the $(\mathrm{BaLi})^+$ system. In Figs. 8(a) and 8(b) we present $\sigma_D^{S,T}$ as a function of energy in log-log scale with base e for the two potentials concerned. The red dashed lines show the Langevin behavior fitted with a slope equal to $-1/2$. We see that at high energies the mean behavior of $\sigma_D^{S,T}$ is close to the Langevin behavior.

V. CONCLUSION

We have studied the collisional properties of the $(\mathrm{BaLi})^+$ IA system which are of particular interest as the experimentally achievable cold Ba^+-Li combination corresponds to the ground asymptote and thereby is protected against radiative

charge transfer loss. We made use of the *ab initio* method to obtain the molecular potentials. We presented a schematic description to study FR with the aim of venturing into the same in the near future by our Wronskian-based multichannel computational method [46]. We calculated the elastic scattering cross section at various regimes of collisional energy and verified its obedience to the semiclassical $(-1/3)$ power law at high energies. We studied the SE collision cross section and compared its energy dependence with the Langevin cross section, which goes well in an expected intermediate-energy regime. We studied the PWPL effect for low partial waves and gave an approximate formula for the SE cross section in the PWPL scenario. Finally, we investigated the diffusion properties of the IA gas system, which obeys the Langevin behavior at high energies. We found that in the ultracold energy or low-energy regime, elastic collisions dominate for $(\mathrm{BaLi})^+$ atom-ion collisions. We note that in such an energy domain, the diffusion cross sections become comparable to elastic cross sections. However, at a relatively high-energy limit, the spin-exchange collisions start to compete with elastic collisions. We hope that our calculated potential energy surfaces, spin-orbit coupling, and scattering analysis can serve as a solid foundation for future studies on the $(\mathrm{BaLi})^+$ system in detail.

[1] J. Weiner, V. S. Bagnato, S. Zilio, and P. S. Julienne, Experiments and theory in cold and ultracold collisions, Rev. Mod. Phys. **71**, 1 (1999).

[2] T. Köhler, K. Góral, and P. S. Julienne, Production of cold molecules via magnetically tunable Feshbach resonances, Rev. Mod. Phys. **78**, 1311 (2006).

[3] L. D. Carr, D. DeMille, R. V. Krems, and J. Ye, Cold and ultracold molecules: Science, technology and applications, New J. Phys. **11**, 055049 (2009).

[4] S. Schmid, A. Härter, and J. H. Denschlag, Dynamics of a Cold Trapped Ion in a Bose-Einstein Condensate, Phys. Rev. Lett. **105**, 133202 (2010).

[5] R. Côté, From Classical Mobility to Hopping Conductivity: Charge Hopping in an Ultracold Gas, Phys. Rev. Lett. **85**, 5316 (2000).

[6] R. Côté, V. Kharchenko, and M. D. Lukin, Mesoscopic Molecular Ions in Bose-Einstein Condensates, Phys. Rev. Lett. **89**, 093001 (2002).

[7] D. Sardar, S. Naskar, A. Pal, H. Berriche, and B. Deb, Formation of a molecular ion by photoassociative raman processes, J. Phys. B **49**, 245202 (2016).

[8] L. Ratschbacher, C. Zipkes, C. Sias, and M. Köhl, Controlling chemical reactions of a single particle, Nat. Phys. **8**, 649 (2012).

[9] L. Ratschbacher, C. Sias, L. Carcagni, J. M. Silver, C. Zipkes, and M. Köhl, Decoherence of a Single-Ion Qubit Immersed in a Spin-Polarized Atomic Bath, Phys. Rev. Lett. **110**, 160402 (2013).

[10] H. Doerk, Z. Idziaszek, and T. Calarco, Atom-ion quantum gate, Phys. Rev. A **81**, 012708 (2010).

[11] H. Ladjimi, D. Sardar, M. Farjallah, N. Alharzali, S. Naskar, R. Mlika, H. Berriche, and B. Deb, Spectroscopic properties of the molecular ions BeX$^+$ (X= Na, K, Rb): Forming cold molecular ions from an ion-atom mixture by stimulated raman adiabatic process, Mol. Phys. **116**, 1812 (2018).

[12] O. P. Makarov, R. Côté, H. Michels, and W. W. Smith, Radiative charge-transfer lifetime of the excited state of (NaCa)$^+$, Phys. Rev. A **67**, 042705 (2003).

[13] A. K. Belyaev, S. A. Yakovleva, M. Tacconi, and F. A. Gianturco, Resonances in Ca$^+$ + Rb nonadiabatic collisions at ultralow energies, Phys. Rev. A **85**, 042716 (2012).

[14] B. McLaughlin, H. Lamb, I. Lane, and J. McCann, Ultracold, radiative charge transfer in hybrid Yb ion–Rb atom traps, J. Phys. B **47**, 145201 (2014).

[15] M. Tomza, C. P. Koch, and R. Moszynski, Cold interactions between an Yb$^+$ ion and a Li atom: Prospects for sympathetic cooling, radiative association, and Feshbach resonances, Phys. Rev. A **91**, 042706 (2015).

[16] M. Farjallah, D. Sardar, N. El-Kork, B. Deb, and H. Berriche, Electronic structure and photoassociation scheme of ultracold (MgK$^+$) molecular ions, J. Phys. B **52**, 045201 (2019).

[17] M. Farjallah, D. Sardar, B. Deb, and H. Berriche, Electronic structure, spectroscopy, cold ion-atom elastic collision properties and photoassociation formation prediction of (MgCs)$^+$ molecular ion, arXiv:2210.01193.

[18] P. Zhang, A. Dalgarno, R. Côté, and E. Bodo, Charge exchange in collisions of beryllium with its ion, Phys. Chem. Chem. Phys. **13**, 19026 (2011).

[19] N. Alharzali, D. Sardar, R. Mlika, B. Deb, and H. Berriche, Spectroscopic properties and cold elastic collisions of alkaline-earth Mg + Mg$^+$ system, J. Phys. B **51**, 195201 (2018).

[20] P. Zhang, A. Dalgarno, and R. Côté, Scattering of Yb and Yb$^+$, Phys. Rev. A **80**, 030703(R) (2009).

[21] M. Cetina, A. T. Grier, and V. Vuletić, Micromotion-Induced Limit to Atom-Ion Sympathetic Cooling in Paul Traps, Phys. Rev. Lett. **109**, 253201 (2012).

[22] H. Fürst, T. Feldker, N. V. Ewald, J. Joger, M. Tomza, and R. Gerritsma, Dynamics of a single ion-spin impurity in a spin-polarized atomic bath, Phys. Rev. A **98**, 012713 (2018).

[23] T. Feldker, H. Fürst, H. Hirzler, N. Ewald, M. Mazzanti, D. Wiater, M. Tomza, and R. Gerritsma, Buffer gas cooling of a trapped ion to the quantum regime, Nat. Phys. **16**, 413 (2020).

[24] P. Weckesser, F. Thielemann, D. Wiater, A. Wojciechowska, L. Karpa, K. Jachymski, M. Tomza, T. Walker, and T. Schaetz, Observation of Feshbach resonances between a single ion and ultracold atoms, Nature (London) **600**, 429 (2021).

[25] C. Ticknor, C. A. Regal, D. S. Jin, and J. L. Bohn, Multiplet structure of Feshbach resonances in nonzero partial waves, Phys. Rev. A **69**, 042712 (2004).

[26] T. Sikorsky, Z. Meir, R. Ben-Shlomi, N. Akerman, and R. Ozeri, Spin-controlled atom-ion chemistry, Nat. Commun. **9**, 920 (2018).

[27] T. Sikorsky, M. Morita, Z. Meir, A. A. Buchachenko, R. Ben-shlomi, N. Akerman, E. Narevicius, T. V. Tscherbul, and R. Ozeri, Phase Locking between Different Partial Waves in Atom-Ion Spin-Exchange Collisions, Phys. Rev. Lett. **121**, 173402 (2018).

[28] H.-J. Werner, P. J. Knowles, G. Knizia, F. R. Manby, and M.Schütz, Molpro A general-purpose quantum chemistry program package, WIREs Comput. Mol. Sci. **2**, 242 (2012).

[29] B. P. Prascher, D. E. Woon, K. A. Peterson, T. H. Dunning, and A. K. Wilson, Gaussian basis sets for use in correlated molecular calculations. VII. Valence, core-valence, and scalar relativistic basis sets for Li, Be, Na, and Mg, Theor. Chem. Acc. **128**, 69 (2011).

[30] J. G. Hill and K. A. Peterson, Gaussian basis sets for use in correlated molecular calculations. XI. Pseudopotential-based and all-electron relativistic basis sets for alkali metal (K–Fr) and alkaline earth (Ca–Ra) elements, J. Chem. Phys. **147**, 244106 (2017).

[31] I. S. Lim, P. Schwerdtfeger, B. Metz, and H. Stoll, All-electron and relativistic pseudopotential studies for the group 1 element polarizabilities from K to element 119, J. Chem. Phys. **122**, 104103 (2005).

[32] R. Yu, A. Kramida, J. Reader, W. Martin, A. Musgrove, E. Saloman, C. Sansonetti, and J. Curry, NIST Atomic Spectra Database, available at https://www.nist.gov/pml/atomic-spectra-database (NIST, Gaithersburg, 2006).

[33] R. W. Molof, H. L. Schwartz, T. M. Miller, and B. Bederson, Measurements of electric dipole polarizabilities of the alkali-metal atoms and the metastable noble-gas atoms, Phys. Rev. A **10**, 1131 (1974).

[34] W. E. Cooke, T. F. Gallagher, R. M. Hill, and S. A. Edelstein, Resonance measurements of d-f and d-g intervals in lithium Rydberg states, Phys. Rev. A **16**, 1141 (1977).

[35] T. M. Miller and B. Bederson, Atomic and molecular polarizabilities—A review of recent advances, Adv. At. Mol. Phys. **13**, 1 (1978).

[36] B. K. Sahoo and B. P. Das, Relativistic coupled-cluster studies of dipole polarizabilities in closed-shell atoms, Phys. Rev. A **77**, 062516 (2008).

[37] E. L. Snow and S. R. Lundeen, Fine-structure measurements in high-L n = 17 and 20 Rydberg states of barium, Phys. Rev. A **76**, 052505 (2007).

[38] B. K. Sahoo, R. G. E. Timmermans, B. P. Das, and D. Mukherjee, Comparative studies of dipole polarizabilities in Sr$^+$, Ba$^+$, and Ra$^+$ and their applications to optical clocks, Phys. Rev. A **80**, 062506 (2009).

[39] M. Śmiałkowski and M. Tomza, Interactions and chemical reactions in ionic alkali-metal and alkaline-earth-metal diatomic AB^+ and triatomic A_2B^+ systems, Phys. Rev. A **101**, 012501 (2020).

[40] A. R. Edmonds, *Angular Momentum in Quantum Mechanics* (Princeton University Press, Princeton, 1996).

[41] R. Côté, in *Advances in Atomic, Molecular, and Optical Physics*, edited by L. F. DiMauro, H. Perrin, and S. F. Yelin (Elsevier, Amsterdam, 2016), Vol. 65, Chap. 2, pp. 67–126.

[42] A. Dalgarno and A. Williams, The second approximation to the mobilities of ions in gases, Proc. Phys. Soc. **72**, 274 (1958).

[43] A. Dalgarno, M. C. McDowell, and A. Williams, The mobilities of ions in unlike gases, Philos. Trans. R. Soc. London Ser. A **250**, 411 (1958).

[44] A. Dalgarno and D. R. Bates, The mobilities of ions in their parent gases, Philos. Trans. R. Soc. London Ser. A **250**, 426 (1958).

[45] E. W. McDaniel and E. A. Mason, *Mobility and Diffusion of Ions in Gases* (Wiley, New York, 1973).

[46] D. Sardar, A. Rakshit, S. Naskar, and B. Deb, Multichannel quantum defect theory with numerical reference functions: Applications to cold atomic collisions, arXiv:2004.09091.